RSC Advances

Repeat-protein mediated synthesis of gold nanoparticles: Effects of protein shape on nanoparticle morphology and optical properties.

Journal:	*RSC Advances*
Manuscript ID:	RA-ART-10-2014-012014.R1
Article Type:	Paper
Date Submitted by the Author:	25-Nov-2014
Complete List of Authors:	Geng, Xi; Virginia Tech, Chemistry Grove, Tijana; Virginia Tech, Chemistry

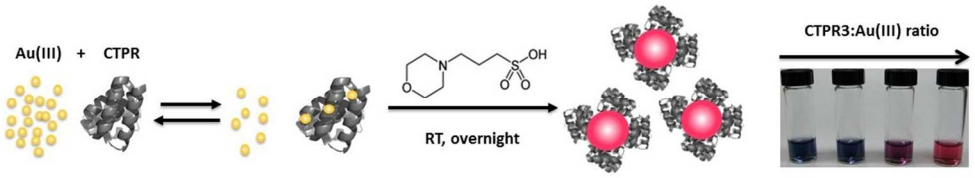

319x67mm (96 x 96 DPI)

Journal Name

RSCPublishing

ARTICLE

Repeat protein mediated synthesis of gold nanoparticles: Effect of protein shape on the morphological and optical properties

Cite this: DOI: 10.1039/x0xx00000x

Received 00th January 2012,
Accepted 00th January 2012

DOI: 10.1039/x0xx00000x

www.rsc.org/

Xi Geng[a] and Tijana Z. Grove[a]

Repeat proteins have recently emerged as promising candidates for the modular design of biohybrid platforms with a high degree of tunability. Consensus sequence tetratricopetide repeat (CTPR) proteins with increasing number of repeats were designed to probe the effects of protein shape on the morphology and resulting physicochemical properties of plasmonic gold nanoparticles. In a synthetic procedure analogous to the biomineralization processes in nature, CTPRs with 3, 6, or 18 tandem repeats were used as both the stabilizing and shape-directing agent. The electronic microscopy and spectroscopic studies indicate that both the $[HAuCl_4]$/[CTPR] ratio and the CTPR shape have dramatic implications on the morphology and plasmon absorbance of the as-synthesized Au NPs. Induced plasmon ellipticity and fluorescence quenching data provide further evidence for the molecular interaction between CTPR and Au NPs or $HAuCl_4$ species. Overall, this work elucidated the effects of CTPR protein shape on the morphology and plasmonic properties of Au NPs, which will further guide the rational design of modular protein based bioconjugate frameworks for colorimetric and enantiomeric biosensors.

Introduction

Over the past few decades, versatile synthetic approaches towards inorganic nanoparticles with well-defined structures and precisely tailored physicochemical properties have been extensively studied and developed.[1] An area of growing interest is the harnessing of biomolecules for the synthesis and assembly of nanoparticles under mild ambient conditions for biosensing and catalysis.[2,3] Bioenabled strategies draw inspiration from nature where materials with unique structures, compositions, and functions are achieved in the process of biomineralization through the interaction of inorganic material with bioscaffold such as peptides[4-10], proteins[11-17] and nucleic acids.[18-24]

In particular, extensive research has focused on the biomimetic synthesis of Au NPs as the fundamental building blocks for the construction of catalytic, optoelectronic and biosensing devices.[12,25,26] To date, a broad spectrum of natural and recombinant proteins were exploited as biotemplates for the synthesis of Au NPs with tailored structures.[11-14,16] In a representative example, anisotropic Au NPs arrays have been integrated on the self-assembled protein clathrin Hub-His6 through a two-step, seed-mediated growth process. In another study, a tetrapod shape was achieved through the coordination of in-situ prepared Au nanoclusters with the trimeric gp5-His6 protein.[11] More recently, proteins were used for the directed growth of highly fluorescent Au nanoclusters with discrete sizes.[27] While these examples illustrate new avenues for the synthesis of inorganic nanoparticles and their assemblies, a thorough understanding of the structure and function of proteins as well as the interactions at the bio-abio interface is key step to tuning the size, shape, composition, and functionality of the final biohybrid nanomaterials.

In this work we exploit designed repeat proteins for bioenabled synthesis of chirooptical Au NPs. Repeat proteins are composed of multiple tandem repeats of small structural motif. Their modular architecture is based on well-defined local interactions between neighbouring repeats. The structure, stability, and function of repeat proteins can be modulated in a predictable manner by simple combination of repeats with desired properties,[28] making this class of proteins especially well-suited for biotechnological applications.

Protein arrays consisting of multiple repeats of the 34 amino acid helix-turn-helix **c**onsensus sequence **t**etratrico**p**eptide **r**epeat, CTPR, have recently emerged as a promising candidates for the modular design of biohybrid platforms with a high degree of tunability.[29-33]

The simplest repeat protein system is one in which all the repeats within a protein are identical, such as the CTPRn protein array, where n stands for the number of tandem repeats. Such CTPRn protein can therefore be treated as a simple homopolymeric molecule, where the monomer is a single repeat helix-turn-helix motif 34 amino acids in length. CTPRn arrays form a superhelical structure, where eight repeats (n=8) comprise one full turn of the superhelix.[35]

The advantage of the modular architecture is that it is possible to design proteins that are chemically identical but differ in size and shape. Herein, we use this property of repeat proteins to explore the effects of protein shape on size distribution, morphology, and plasmonic optical properties of Au NPs. Although much is known about how protein and peptide primary sequences affect the nucleation and growth of Au NPs,[8] the influence of protein structure and shape is not well understood. To this end, we engineered CTPRn arrays, where n= 3, 6, or 18, with identical surface chemistry, but distinct shapes expressed as aspect ratio (***Figure 1c***). These proteins were then used in the one-step synthesis of CTPR-Au NPs conjugates.

In this report, we present a green synthesis strategy for the fabrication of repeat protein-stabilized Au NPs. CTPR proteins with varied number of repeating units were employed as both the stabilizer and structure-directing agent for the construction of protein-Au NPs conjugates. Direct interactions between protein and Au precursor were observed in fluorescence quenching experiments. The shape and particle size of Au NPs is closely correlated to the concentration and the length of CTPRn array as seen in TEM images.

Accordingly, the plasmon absorption of the resultant CTPR-stabilized Au NPs could be tuned spanning a wide wavelength range. Circular dichroism analysis further demonstrated that CTPR proteins retained their secondary structure after conjugation with Au NPs. Interestingly, induced chirality was also detected in the region of the plasmonic absorption of CTPR-Au NPs.

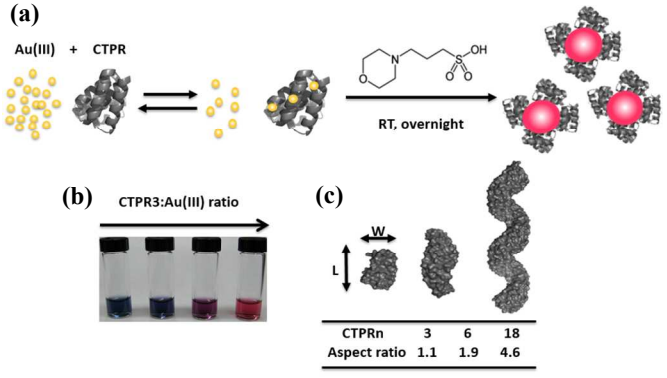

Figure 1. (a) Schematic illustration of the synthesis of CTPR stabilized Au NPs. Gold precursor ions are mixed with CTPR protein at predefined concentration ratios followed by the addition of the reducing agent. (b) Photograph of CTPR3 stabilized Au colloids. Localized surface plasma resonance (LSPR) blue-shifts with increasing [CTPR3]:[Au(III)] ratio. (c) Cartoon representation of CTPR3, 6 and 18 with different aspect ratios but identical surface residues. This cartoon was prepared from X-ray coordinates[35] using Pymol. (http://www.pymol.org/)

Experimental

Chemicals

Chloroauric acid (99.9%) was purchased from Strem Chemicals Inc. 3-(N-morpholino)propanesulfonic acid (MOPS) were acquired from MP biomedicals, LLC. Other reagents were purchased from Sigma-Aldrich and Fisher Chemicals. All reagents were used as received without further purification. Deionized water (18MΩ/cm, Millipore Milli-Q) was exclusively used for preparing all aqueous solutions and for all the rinsing procedures.

Expression of CTPR proteins

CTPR proteins with 3, 6 and 18 tandem repeating units were synthesized through recombinant bacterial expression technology as described previously (***Figure S1***).[29,31] Synthetic genes for the desired protein in pPROEx vector, coding for N-terminal $(His)_6$ tag and ampicillin resistance, were transformed into E.Coli BL21(DE3) cells and cultured overnight at 37°C on agar plates. One single colony was selected and incubated overnight in 50 mL of Luria−Bertani (LB) media containing 100 µg/mL of ampicillin. 10ml of overnight cultures were then dispensed into 1 L of LB media supplemented with 100 µg/mL ampicillin. The cells were grown in an incubator-shaker (250rpm) at 37 °C until the optical density (OD_{600}) reached 0.6-0.8. Expression of CTPR3 was induced with 1mM isopropyl β-D-thiogalactoside (IPTG) followed by 5h expression at 37°C, whereas CTPR6 and 18 were expressed at 18°C for 16h in an analogous manner. The cells were harvested by centrifugation at 5,000rpm for 20min and the pellets were frozen at -80°C until purification.

Purification of CTPR proteins

The cell pellets were resuspended in lysis buffer consisting of 50 mM Tris, 300mM sodium chloride and 0.1wt% Tween 20. After 2 min sonication at 30% power using a microtip and Mison sonicator, lysed cells were centrifuged at 16,000 rpm for 30 min and the protein supernatant was purified using standard Ni-NTA affinity purification protocol. The N-terminal hexahistidine tag was then cleaved from the CTPR proteins using TEV protease. The collected proteins were further purified by Akta Prime Plus size exclusion chromatography using Superdex 75 16/600 or 200 16/600 Prep Grade column in 150mM sodium chloride and 50mM sodium phosphate buffer at pH 8 with a flow rate of 0.5ml/min. As a final step, the aqueous solutions of CTPRs were dialyzed against 10mM phosphate buffer three times at 4 °C using a dialysis membrane with molecular weight cutoff of 3k or 10kDa.

Preparation of CTPR-stabilized gold nanoparticles

The protein-Au NP conjugates were synthesized via the approach depicted in ***Figure 1a***. In a typical procedure, 100µl of 10mM phosphate buffer solution of CTPRn was added into 0.5ml of 0.4mM aqueous solution of chloroauric acid. Subsequently, 0.4ml of

100mM MOPS pH 7.4 was added to the solution at ambient conditions. A series of CTPR-Au NPs samples were prepared in the same way where the concentration of $HAuCl_4$ and MOPS was held constant, while the ratio of [$HAuCl_4$]/ [CTPR] was adjusted to 1000, 400, 100 and 20. The samples are denoted as CTPRn-Au-m, where n is the number of tandem CTPR repeats and m is the ratio of [$HAuCl_4$]/[CTPR] (n=3,6,18; m=1k, 400, 100, 20).

Instrumentations

The transmission electron microscopy (TEM) analysis was performed on a Philips EM420 at an accelerating voltage of 120kV. TEM samples were prepared by applying a 7µl sample solution on 300 mesh carbon-coated Cu grids (EM Science), followed by drying overnight before observation. The particle-size distribution was estimated by measuring the size of approximately 100 NPs at different regions using Image J.

The UV-Vis spectra of CTPR-Au NPs were monitored using an Agilent Cary 100 Bio UV-Vis spectrophotometer. All UV-vis measurements were conducted in 1cm path length quartz cuvette at room temperature. The fluorescence quenching experiments were carried out at room temperature and 50°C on an Agilent Cary Eclipse fluorimeter using the 1cm path length quartz cuvette. Briefly, 2µM CTPR3 protein was titrated every 10min with 2µl of 2mM $HAuCl_4$ aqueous solution.

Circular dichroism data were acquired using samples containing 0.5-2µM protein on a Jasco J-815 CD spectrometer. Far UV CD (190nm-280nm) spectra were recorded at 25°C to assess the secondary structure of CTPR proteins. Each sample was recorded three times from 190-260nm in a 2mm pathlength quartz cuvette, and averaged. Data were collected using a 1 nm bandwidth, 2 nm data pitch, and a data integration time of 1 s. The CD intensities are expressed in terms of [θ] and were normalized to units of mean residue ellipticity for all samples (deg*cm^2*dmol^{-1}). The induced chirality of CTPR-Au samples was recorded by monitoring the ellipticity in the visible region (400nm-650nm) using a 10mm pathlength cuvette.

Results and discussion

Design and construction of CTPR stabilized Au NPs

Our strategy for repeat-protein enabled synthesis of Au NPs is illustrated in ***Figure 1***. In this work we exploit the modular construction of CTPR proteins to explore the effects of protein shape and concentration on size distribution and morphology of plasmonic Au NPs. CTPRn arrays are composed of tandem repeats of a basic structural unit, 34 amino acids in length. In contrast to globular proteins, repeat proteins have no interactions between residues at large distance in the primary structure, which makes them much easier to engineer. The stability of individual CTPR units can be rationally manipulated, and the stability of CTPRn arrays can be predicted based on the behavior of the units from which they are composed.[27,30] This unprecedented level of control and predictability of both the structure and thermodynamic stability means that CTPR units can be mixed and matched in a modular and predetermined fashion to design proteins with the desired properties.[36] CTPRn arrays (n=3, 6, or 18, ***Figure 1c***) were used in one-pot synthesis of Au NP under ambient conditions. This synthetic scheme in ***Figure 1a*** is analogous to the typical biomineralization process in nature where the metal ions are first sequestered with a bioscaffold at predefined concentration ratios. As observed in photographs in Figure 1b, plasmonic Au NP colloid are formed upon addition of a mild reducing agent, MOPS.

In a typical protein-directed synthesis, Au ions are reduced either by a strong reducing agent or by the reductive functional groups in proteins which are typically activated by increasing the pH of the solutions to alkaline. [11,27] However, the harsh reaction conditions involved in these processes often lead to an irreversible conformational change of the proteins.[37] A milder synthetic method is therefore required to preserve the structure of the proteins in the protein-directed approach. Notably, the use of Good's buffers has been explored for Au NPs synthesis that could be performed under extremely mild conditions. [15,38-41] This is crucial for one-step synthesis and functionalization of NPs with biomolecules that often do not tolerate organic solvents, wide pH range, and elevated temperatures. In the absence of CTPR protein, flower-like Au nanoparticles were generated using MOPS as the reducing agent (***Figure 2a***). The mean particle size was estimated to be 33.3±9.7nm. It has been observed previously that the tertiary amine of either the piperazine or the morpholine group is capable of reducing the metal ions through formation of nitrogen centered radicals.[41] Despite the reports that piperazine ring is essential for the surface ligand mediated growth of highly branched nanoparticles,[38] it is evident from our data that the morpholine group serves as a shape-directing agent to promote the agglomeration of primary Au seeds and the ensuing branched NP growth.

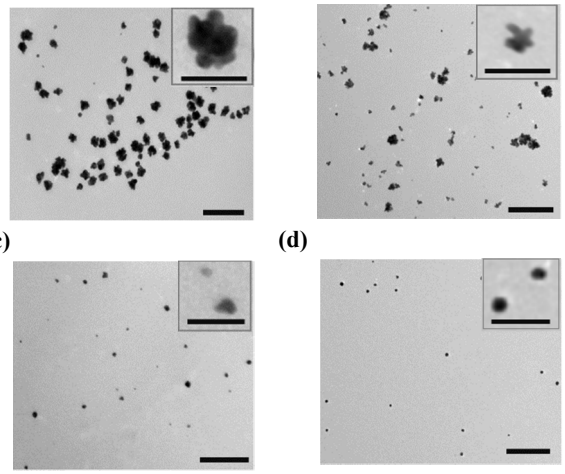

Figure 2. TEM images. Au NPs synthesized as described using [$HAuCl_4$]=0.2mM and (a)no CTPR3 added (b) CTPR3-Au-1k (c) CTPR3-Au-100 (d) CTPR3-Au-20. (Scale bar =200nm) Inset: magnified TEM images with scale bar=50nm.

The TEM images of CTPR3-stabilized Au NPs prepared with different [$HAuCl_4$]/[CTPR3] ratios in MOPS buffer are shown in the ***Figure 2b-d.*** In the presence of the low concentration of CTPR3, branched or multipod-like Au NPs were produced (***Figure 2b***). As the concentration of protein increases, nanoparticles become less agglomerated and more spherical (***Figure 2d***). We speculate that the Au(III) ions are coordinated by the protein surface residues to form stable CTPR3-$HAuCl_4$ complexes thereby providing potential nucleation sites for the in-situ reduction of Au by MOPS. Subsequently, the growth of Au NPs is partially suppressed by capping the Au core with CTPR3 corona. However, the excess amount of Au(III) ions located in the vicinity of the initial Au-CTPR3 complex favors the rapid growth of individual Au NPs as well as the inevitable aggregation of adjacent small Au NPs formed at the initial stage of the reaction. Although the mean particle size does not change dramatically as a function of protein concentration, the size distribution becomes much narrower (***Figure 3***). Agglomerated nanoclusters and highly branched NPs gradually disappeared, whereas the Au polyhedron and nanospheres are produced as CTPR3 concentration increases. We propose that increasing the amount of CTPR3 depletes the Au(III) at individual nucleation sites and hampers the overgrowth of Au NPs. In addition, CTPR protein also acts as an efficient stabilizer to inhibit the secondary nucleation and the agglomeration of Au NPs. It is noteworthy that CTPR3 template does not contain cysteine (thiols) or histidine (imidazole) residues that have been previously observed to bind metal NP surfaces.[42,43] However, Hill et al. reported that resilin-mimetic protein uses tyrosine (Tyr) residues for organization of AuNPs on its surface.[16] Recent molecular dynamics simulations also revealed strong binding affinity of Tyr for Au NPs.[44] Thus we reasoned that CTPR protein, where each repeat contains seven aromatic Tyr and one tryptophan (Trp) residues, will interact with gold species during the biomimetic synthesis. To gain more insight into the molecular level interactions of CTPRn arrays and gold, we have performed fluorescence quenching experiments.

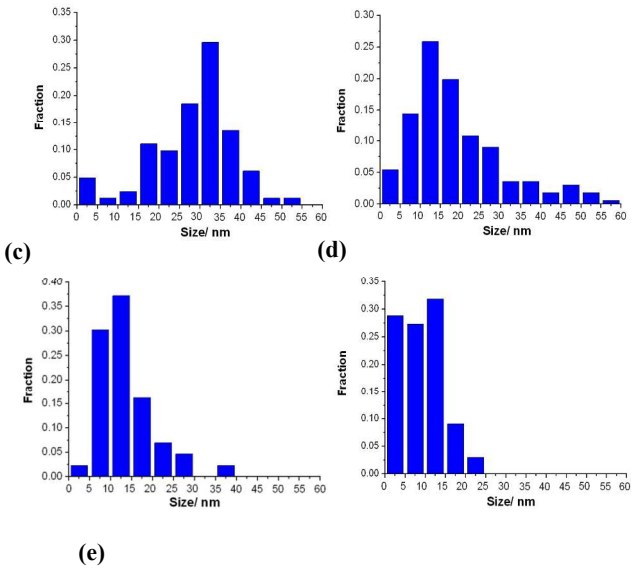

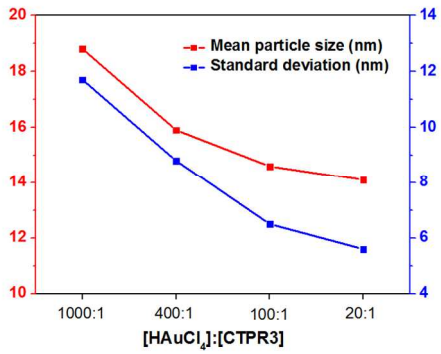

Figure 3. Histograms of the size distribution of (a) Au NPs in the absence of CTPR3 (b) CTPR3-Au-1k (c) CTPR3-Au-100 (d) CTPR3-Au-20 (e) Mean particle size and standard deviation of CTPR3-Au NPs .

Molecular interaction between CTPR and Au(III) and Au NPs

Each CTPR repeat contains seven tyrosine and one tryptophan for total of 21, 42, and 126 surface-exposed aromatic residues for CTPR3, CTPR6, and CTPR18 respectively. Thus all CTPR proteins exhibit excitation and emission peaks at 275 and 338nm respectively. Conveniently, these aromatic side-chains are built-in fluorescent probes of protein-ligand interactions. The pronounced quenching of CTPR3 fluorescence (***Figure 4a***) confirms that both Au(III) ions and Au NP interact with the protein surface, consistent with the proposed reaction scheme in ***Figure 1a***. To closer inspect the molecular mechanism of fluorescence quenching, we titrated Au(III) ions into the solution of CTPR3 and observed fluorescence quenching as a function of Au(III) concentration ***Figure 4b.*** The fluorescence signal was corrected due to the inner filter effect by multiplying the observed fluorescence F_{obs} with appropriate factors as shown in the equation:

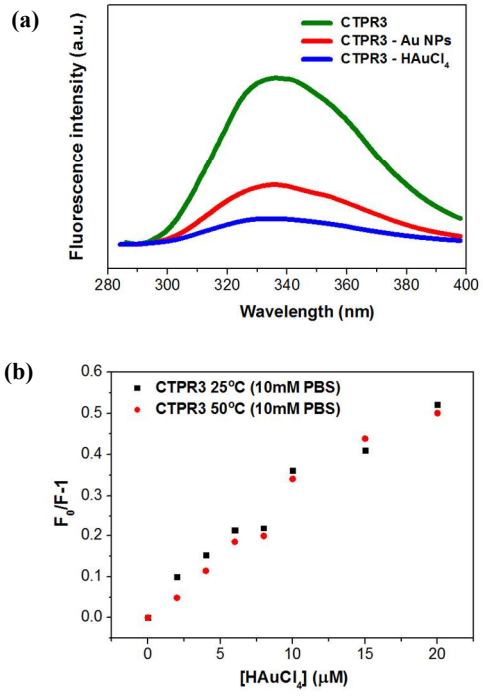

Figure 4. Fluorescence spectra of (a) CTPR3, CTPR3-$HAuCl_4$(100:1), CTPR3-Au-100 colloidal solution (b) Corrected fluorescence quenching profile of CTPR3 by $HAuCl_4$ in 10mM PBS at 25°C and 50°C. (Error bars are smaller than symbols.)

Because CTPR proteins are stable under a relatively broad range of temperatures,[28] we can readily change the solution conditions to further probe binding of Au(III) to CTPR. To distinguish between a collisional and static mechanism of fluorescence quenching, we performed identical titration experiments at room temperature and 50°C. For a purely collisional mechanism of fluorescence quenching we expected to observe a steeper quenching curve due to the faster diffusion rate at elevated temperatures. Conversely, for purely static fluorescence quenching, the quenching curve will have a flattened slope arising from the dissociation of weekly bound fluorophore-quencher complex at elevated temperatures.[46] The slope of the quenching curve does not change with the temperature implying that the interaction of Au(III) with CTPR could be explained by a combination of static and dynamic quenching.

$$\boldsymbol{F_{ideal}(\lambda_{ex},\ \lambda_{em}) = F_{obs}(\lambda_{ex},\ \lambda_{em})CF_p(\lambda_{ex})CF_s(\lambda_{em}) = F_{obs}(\lambda_{ex},\ \lambda_{em})10^{(A_{ex}+A_{em})/2}} \quad (1)$$

where CF_p , CF_s represents the correction factors for the total absorbance A_{ex} and emission A_{em} at the wavelength of λ_{ex}, λ_{em}, respectively.[45]

The Stern-Volmer quenching constant, $K_{SV,}$ was estimated to be $2.7*10^4$ M^{-1} by fitting the data in ***Figure 4b*** to equation (2). Approximating that the fluorescence lifetime, $\tau_{0,}$ for biomacromolecules is around $5*10^{-9}$ s,[16] the bimolecular quenching constant, $k_{q,}$ for CTPR3 and Au(III) ions was calculated to be $5.3*10^{12}M^{-1}s^{-1}$. This value is two orders of magnitude higher than $2*10^{10}$ $M^{-1}s^{-1}$ for a typical diffusion controlled quenching process consistent with the formation of the complex between CTPR3 and Au(III) species.

$$\boldsymbol{\frac{F_0}{F} = 1 + K_{SV}[Q], \qquad K_{SV} = k_q\tau_0} \quad (2)$$

Effects of increasing length of CTPRn array on the growth and optical properties of Au NPs

One may make an argument that extending a protein sequence could simply increase the number of Au binding sites. Indeed, studies of the mechanism and kinetics of NP formation using tyrosine-based oligopeptides clearly showed that with increasing number of amino acid residues, the size of the NPs increased and polydispersity decreased.[45] However, the relationship between protein length and morphologies of NPs is more elusive. For this purpose, CTPR arrays with increasing numbers of repeats were used in the synthesis of Au NPs. Previous hydrodynamic studies of CTPR arrays established that these proteins behave as rigid rods in solution, i.e. their molecular dimensions in solutions are identical to that observed in the high-resolution crystal structure.[34] Thus we will describe the protein shape with the aspect ratio calculated from the X-ray coordinates.[35]

Increasing the protein concentration in the reaction mixture results in a transition of NP morphology from larger branched aggregates

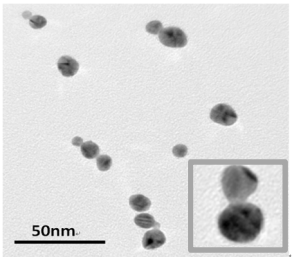

towards smaller globular particles regardless of CTPR array aspect ratio (***Figure 2S***). However, distinct oligometric nanostructures including fused dimer and trimers are observed for CTPR6-Au-20 samples (***Figure 5***). These morphologies were not observed in the presence of same concentration of CTPR3 or CTPR18. This result implies that CTPR6 may serve as a scaffold for the controlled arrangement of one-dimensional nanostructures analogous to what has been previously achieved with the DNA origami.[18,20,21] Additionally, we also observed that further increase in the concentration of the total amount of CTPR repeat does not lead to the smaller particle size and narrower size distribution for CTPR18-Au-100 as compared to CTPR3-Au-100, and CTPR6-Au-100 (***Table S2***).

Figure 5. CTPR6-Au-20 oligomers. (Inset: magnified image of fused CTPR-Au NPs).

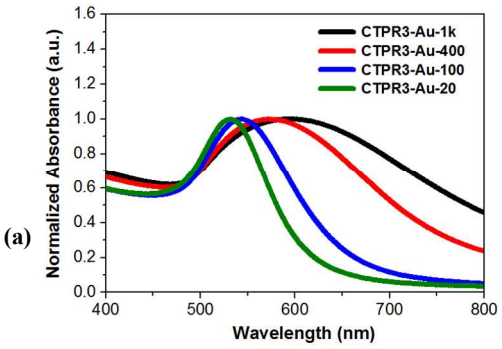

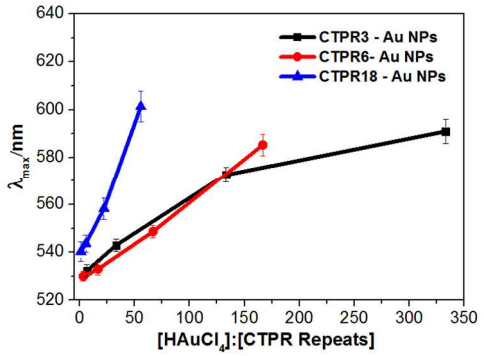

Figure 6. (a) Normalized UV-vis spectra of Au NPs synthesized in the presence of CTPR3: CTPR3-Au-1k, CTPR3-Au-400, CTPR3-Au-100 and CTPR3-Au-20 NPs (b) Maximum plasmon absorption wavelength of CTPR-AuNPs as a function of [$HAuCl_4$]/[CTPR] and (c) as a function of [$HAuCl_4$]/[number of CTPR repeats]. (e.g. the concentration of [number of CTPR repeats] equals 3 fold of [CTPR3], since each CTPR3 protein is composed of 3 repeats.)

UV-vis spectroscopy was used to monitor the surface plasmon resonance band of CTPR-Au NP. A remarkable bathochromic shift was observed as the protein concentration decreases (***Figure 6***). For instance, CTPR3-Au-1k displayed a wavelength of maximum absorbance λ_{max} at 591nm. Upon the addition of an increased amount of CTPR3, the λ_{max} changed to 532nm for CTPR3-Au-20, which is the characteristic absorption of spherical Au NPs. It is well-established that the longitudinal localized surface plasmon resonance (LSPR) is determined by the size as well as the aspect ratio of anisotropic NPs.[48,49] The substantial LSPR red-shift for Au prepared in the presence of low concentration of CTPR could be ascribed to the morphological features such as elongated shapes, branched tips, etc.[38] This result is in good agreement with the representative TEM images showing branched or agglomerated morphologies at low protein concentrations. Likewise, the λ_{max} of CTPR6 or CTPR18 capped Au followed a similar concentration dependence trend. As shown in ***Figure 6a-b***, ***S3***, narrower SPR peaks and substantial decrease in λ_{max} were obtained when the Au NPs were prepared under the condition of low [$HAuCl_4$]/[CTPR] ratio, i.e. increased protein concentration.

We further investigated the influence of the protein aspect ratio on the SPR of Au NPs by plotting the λ_{max} as a function of the ratio of [$HAuCl_4$]/[CTPR repeats]. If variation in morphology and UV-vis spectra are due only to increased number of nucleation sites, we expect the normalized data to follow an identical concentration trend for CTPR3, CTPR6, and CTPR18. Remarkably, two different trends were identified. As seen in the ***Figure 6c***, λ_{max} is more sensitive to the protein concentration for CTPR18 in comparison with CTPR3 and CTPR6. This SPR shift dependence for CTPR18-Au may be correlated to the large aspect ratio of 4.6 and the elongated superhelical structure adopted by CTPR18.[30] We propose that more spherical CTPR3 and 6, aspect ratio of 1.1 and 1.9 respectively, are anchored in a more efficient manner onto the surface of Au NPs to suppress rapid growth and aggregation.

Long term colloidal stability of CTPR-stabilized Au NPs

The colloidal stability of the CTPR-decorated Au NPs was evaluated by monitoring the UV-vis spectra of CTPR3-Au-100 samples placed at 4°C for 3 months. As shown in the ***Figure S4a,*** only a minor loss in the LSPR intensity was identified whereas no noticeable shift or broadening of LSPR peak occurred. In addition, TEM analysis also confirmed that the Au NPs were well-dispersed and no self-aggregation behavior was found for the CTPR3-Au-100 sample (***Figure S4b***). Thus, CTPR proteins stabilized Au NPs exhibited remarkably high colloidal stability in MOPS buffer.

Circular dichroism measurements

CTPRn arrays displayed the characteristic CD spectrum of an α-helical protein, with minimum at 222 nm and 208 nm (***Figure 7a).*** The mean residue ellipticity (MRE) remains nearly constant upon addition of $HAuCl_4$ or addition of MOPS. More importantly, no signals characteristic of β-sheet or random coil structures were identified in the CD spectrum. This result suggests that the metal ion coordination does not cause distortion of the secondary structure implying that the bioactivity of CTPR could be kept intact during the Au NP synthesis and finally when bound to the nanoparticle surface.

In addition, the complexation of Au NPs with CTPR-3,6,18 induced a CD response at the plasmon resonance frequency region (ca. 550nm) as shown in the ***Figure 7b.*** As suggested previously,[50] the optical activity of Au NPs capped with chiral ligands is generally attributed to three reasons: (1) in-situ formation of an intrinsic chiral Au nanocluster in the presence of chiral ligands (2) electronic interaction between the chiral ligands and achiral metal core electrons, and (3) chiral arrangement of the ligands on an achiral metal core. Since the plasmonic CD bands of CTPR-Au NPs disappear after ligand exchange with achiral 2-mercaptoethanol, we ruled out in-situ formation of chiral Au nanocluster. We surmise that the negative ellipticity of CTPR-Au NPs complex in the visible spectrum region may result from the dipolar interaction between chiral protein ligands and the plasmonic NPs.[49,51] Induced CD signals at the plasmonic absorption region have been previously demonstrated for peptides with specific Au binding affinity.[6] Exploration of CTPR-Au NPs for the development of biosensors based on the plasmonic chirality is currently underway in our group. It is however important to note that the application of these functionalized NPs is confined to aqueous solutions with physiological pH and ambient conditions. Further studies of the environmental impacts on the stability and optical properties of CTPR-Au NPs will further elucidate advantages and limits of this system.

(a)

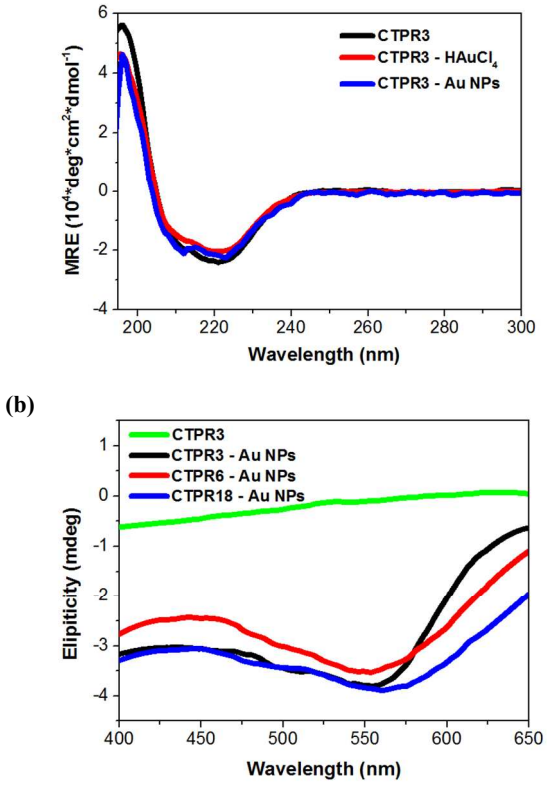

Figure 7. CD spectra of (a) CTPR3CTPR3-HAuCl$_4$(1:100), CTPR3-Au-100 (blue line) in the far UV region and (b) CTPR3 control, CTPR3-Au-100, CTPR6-Au-100 and CTPR18-Au-100 samples in the visible light region.

Conclusions

In summary, we have developed a green-chemistry route for the preparation of Au NPs using Good's buffer and modular repeat proteins. TEM and UV-vis analysis indicated that the morphology as well as the LSPR absorbance of Au NPs can be adjusted by varying the ratio of [HAuCl$_4$]/[CTPR] in conjunction with the protein length. This study exemplifies the pivotal role of protein shape in tuning the morphology-dependent optical properties of protein-stabilized Au NPs. CD spectroscopic studies suggested that CTPR retained its secondary structure after coordinating with Au(III) or Au NPs. Moreover, the obtained CTPR-Au conjugates exhibited chirality in the visible light region indicating the strong molecular interaction between the CTPR proteins and Au NPs. This repeat protein-directed synthetic method enabled the facile fabrication of Au NPs with tailored morphology, LSPR and optical activity and may find potential applications in chiral biosensing and catalysis.

Acknowledgements

The authors would like to thank Nanoscale Characterization and Fabrication Lab (NCFL) for the use of TEM facility. We are grateful to Prof. Aitziber L. Cortajarena for insightful comments and suggestions. We acknowledge members of Grove's group for useful discussion of the manuscript. This work was in part supported by the JFC grants from Institute for Critical Technology and Applied Sciecne (ICTAS), Virginia Polytechnic Institute and State University.

Notes and references

[a] *Department of Chemistry, Virginia Polytechnic Institute and State University, Blacksburg, VA 24060, USA. Email: tijana.grove@vt.edu.*
Electronic Supplementary Information (ESI) available.

1 Saha, K.; Agasti, S. S.; Kim, C.; Li, X.; Rotello, V. M. *Chemical Reviews* **2012**, *112*, 2739
2 Dickerson, M. B.; Sandhage, K. H.; Naik, R. R. *Chemical Reviews* **2008**, *108*, 4935.
3 Delehanty, J. B.; Bradburne, C. E.; Susumu, K.; Boeneman, K.; Mei, B. C.; Farrell, D.; Blanco-Canosa, J. B.; Dawson, P. E.; Mattoussi, H.; Medintz, I. L. *Journal of the American Chemical Society* **2011**, *133*, 10482.
4 Naik, R. R.; Stringer, S. J.; Agarwal, G.; Jones, S. E.; Stone, M. O. *Nat Mater* **2002**, *1*, 169.
5 Dickerson, M. B.; Jones, S. E.; Cai, Y.; Ahmad, G.; Naik, R. R.; Kröger, N.; Sandhage, K. H. *Chemistry of Materials* **2008**, *20*, 1578.
6 Slocik, J. M.; Govorov, A. O.; Naik, R. R. *Nano Letters* **2011**, *11*, 701.
7 Chen, C.-L.; Rosi, N. L. *Journal of the American Chemical Society* **2010**, *132*, 6902.
8 Song, C.; Zhao, G.; Zhang, P.; Rosi, N. L. *Journal of the American Chemical Society* **2010**, *132*, 14033.
9 Diamanti, S.; Elsen, A.; Naik, R.; Vaia, R. *The Journal of Physical Chemistry C* **2009**, *113*, 9993.
10 Li, Y.; Tang, Z.; Prasad, P. N.; Knecht, M. R.; Swihart, M. T. *Nanoscale* **2014**, *6*, 3165.
11 Ueno, T.; Koshiyama, T.; Tsuruga, T.; Goto, T.; Kanamaru, S.; Arisaka, F.; Watanabe, Y. *Angewandte Chemie International Edition* **2006**, *45*, 4508.
12 Niide, T.; Shimojo, K.; Wakabayashi, R.; Goto, M.; Kamiya, N. *Langmuir* **2013**, *29*, 15596.
13 Hom, N.; Mehta, K. R.; Chou, T.; Foraker, A. B.; Brodsky, F. M.; Kirshenbaum, K.; Montclare, J. K. *Journal of Materials Chemistry* **2012**, *22*, 23335.
14 Lin, Y.; Xia, X.; Wang, M.; Wang, Q.; An, B.; Tao, H.; Xu, Q.; Omenetto, F.; Kaplan, D. L. *Langmuir* **2014**, *30*, 4406.
15 McMillan, R. A.; Howard, J.; Zaluzec, N. J.; Kagawa, H. K.; Mogul, R.; Li, Y.-F.; Paavola, C. D.; Trent, J. D. *Journal of the American Chemical Society* **2005**, *127*, 2800.
16 Mayavan, S.; Dutta, N. K.; Choudhury, N. R.; Kim, M.; Elvin, C. M.; Hill, A. J. *Biomaterials* **2011**, *32*, 2786.
17 Schoen, A. P.; Schoen, D. T.; Huggins, K. N. L.; Arunagirinathan, M. A.; Heilshorn, S. C. *Journal of the American Chemical Society* **2011**, *133*, 18202.
18 Lan, X.; Chen, Z.; Liu, B.-J.; Ren, B.; Henzie, J.; Wang, Q. *Small* **2013**, *9*, 2308.
19 Tan, L. H.; Xing, H.; Chen, H.; Lu, Y. *Journal of the American Chemical Society* **2013**, *135*, 17675.

20 Zhao, Y.; Xu, L.; Liz-Marzán, L. M.; Kuang, H.; Ma, W.; Asenjo-García, A.; García de Abajo, F. J.; Kotov, N. A.; Wang, L.; Xu, C. *The Journal of Physical Chemistry Letters* **2013**, *4*, 641.

21 Tan, S. J.; Campolongo, M. J.; Luo, D.; Cheng, W. *Nat Nano* **2011**, *6*, 268.

22 Schreiber, R.; Luong, N.; Fan, Z.; Kuzyk, A.; Nickels, P. C.; Zhang, T.; Smith, D. M.; Yurke, B.; Kuang, W.; Govorov, A. O.; Liedl, T. *Nat Commun* **2013**, *4*.

23 Lo, P. K.; Karam, P.; Aldaye, F. A.; McLaughlin, C. K.; Hamblin, G. D.; Cosa, G.; Sleiman, H. F. *Nat Chem* **2010**, *2*, 319.

24 Nykypanchuk, D.; Maye, M. M.; van der Lelie, D.; Gang, O. *Nature* **2008**, *451*, 549.

25 Zou, L.; Qi, W.; Huang, R.; Su, R.; Wang, M.; He, Z. *ACS Sustainable Chemistry & Engineering* **2013**, *1*, 1398.

26 Mahal, A.; Khullar, P.; Kumar, H.; Kaur, G.; Singh, N.; Jelokhani-Niaraki, M.; Bakshi, M. S. *ACS Sustainable Chemistry & Engineering* **2013**, *1*, 627.

27 Xie, J.; Zheng, Y.; Ying, J. Y. *Journal of the American Chemical Society* **2009**, *131*, 888.

28 Cortajarena, A. L.; Regan, L. *Protein Science* **2011**, *20*, 336.

29 Kajander, T.; Cortajarena, A. L.; Main, E. R. G.; Mochrie, S. G. J.; Regan, L. *Journal of the American Chemical Society* **2005**, *127*, 10188.

30 Grove, T. Z.; Osuji, C. O.; Forster, J. D.; Dufresne, E. R.; Regan, L. *Journal of the American Chemical Society* **2010**, *132*, 14024.

31 Cortajarena, A. L.; Yi, F.; Regan, L. *ACS Chemical Biology* **2008**, *3*, 161.

32 Grove, T. Z.; Regan, L.; Cortajarena, A. L. *Journal of The Royal Society Interface* **2013**, *10.*

33 Mejias, S. H.; Sot, B.; Guantes, R.; Cortajarena, A. L. *Nanoscale* **2014.**

34 Cortajarena, A. L.; Lois, G.; Sherman, E.; O'Hern, C. S.; Regan, L.; Haran, G. *Journal of Molecular Biology* **2008**, *382*, 203.

35 Kajander, T.; Cortajarena, A. L.; Mochrie, S.; Regan, L. *Acta Crystallographica Section D* **2007**, *63*, 800.

36 Grove, T. Z.; Forster, J.; Pimienta, G.; Dufresne, E.; Regan, L. *Biopolymers* **2012**, *97*, 508.

37 Yu, Y.; Luo, Z.; Teo, C. S.; Tan, Y. N.; Xie, J. *Chemical Communications* **2013**, *49*, 9740.

38 Xie, J.; Lee, J. Y.; Wang, D. I. C. *Chemistry of Materials* **2007**, *19*, 2823.

39 Xie, J.; Zhang, Q.; Lee, J. Y.; Wang, D. I. C. *ACS Nano* **2008**, *2*, 2473.

40 Park, J.; Choi, S.; Kim, T.-I.; Kim, Y. *Analyst* **2012**, *137*, 4411

41 So, M.-H.; Ho, C.-M.; Chen, R.; Che, C.-M. *Chemistry – An Asian Journal* **2010**, *5*, 132240.

42 Aldeek, F.; Safi, M.; Zhan, N.; Palui, G.; Mattoussi, H. *ACS Nano* **2013**, *7*, 10197.

43 Hou, J.; Szaflarski, D. M.; Simon, J. D. *The Journal of Physical Chemistry B* **2013**, *117*, 4587.

44 Yu, J.; Becker, M. L.; Carri, G. A. *Langmuir* **2011**, *28*, 1408.

45 Zhao, X.; Liu, R.; Chi, Z.; Teng, Y.; Qin, P. *The Journal of Physical Chemistry B* **2010**, *114*, 5625

46 Lakowicz, J. R. *Principles of Fluorescence Spectroscopy; Springer: Singapor,* **2006**.

47 Si, S.; Bhattacharjee, R. R.; Banerjee, A.; Mandal, T. K. *Chemistry – A European Journal* **2006**, *12*, 1256.

48 Nikoobakht, B.; El-Sayed, M. A. *Chemistry of Materials* **2003**, *15*, 1957.

49 Link, S.; El-Sayed, M. A. *The Journal of Physical Chemistry B* **1999**, *103*, 4212.

50 Schaaff, T. G.; Whetten, R. L. *The Journal of Physical Chemistry B* **2000**, *104*, 2630.

51 Govorov, A. O. *The Journal of Physical Chemistry C* **2011**, *115*, 7914.